Biocatalytic enantioselective C(sp^3)–H fluorination enabled by directed evolution of nonheme Fe enzymes

Liu-Peng Zhao[1], Binh Khanh Mai[2], Lida Cheng[1], Fangqiu Gao[1], Yunlong Zhao[1], Rui Guo[1], Hao Wu[3], Yongda Zhang[3], Peng Liu[2]* and Yang Yang[1,4]*

[1] Department of Chemistry and Biochemistry, University of California, Santa Barbara, California 93106, USA

[2] Department of Chemistry, University of Pittsburgh, Pittsburgh, Pennsylvania 15260, USA

[3] Chemical Development, Boehringer Ingelheim Pharmaceuticals, Inc., 900 Ridgebury Road, Ridgefield, Connecticut 06877, USA

[4] Biomolecular Science and Engineering (BMSE) Program, University of California, Santa Barbara, California 93106, USA

*E-mail: pengliu@pitt.edu; yang@chem.ucsb.edu

Owing to the scarcity of C–F bond forming enzymatic reactions in nature and the contrasting prevalence of organofluorine moieties in bioactive compounds, developing biocatalytic fluorination reactions represents a preeminent challenge in enzymology, biocatalysis, and synthetic biology. Additionally, catalytic enantioselective C(sp^3)–H fluorination remains a challenging problem facing synthetic chemists. Although many nonheme Fe halogenases have been discovered to promote C(sp^3)–H halogenation reactions, efforts to convert these Fe halogenases to fluorinases have remained unsuccessful. Here, we report the development of an enantioselective C(sp^3)–H fluorination reaction, catalysed by a plant-derived nonheme enzyme 1-aminocyclopropane-1-carboxylic acid oxidase (ACCO), which is repurposed for radical rebound fluorination. Directed evolution afforded a C(sp^3)–H fluorinating enzyme $ACCO_{CHF}$ displaying 200-fold higher activity, substantially improved chemoselectivity and excellent enantioselectivity, converting a range of substrates into enantioenriched organofluorine products. Notably, almost all the beneficial mutations were found to be distal to the Fe centre, underscoring the importance of substrate tunnel engineering in nonheme Fe biocatalysis. Computational studies reveal that the radical rebound step with the Fe(III)–F intermediate has a low activation barrier of 3.4 kcal mol^{-1} and is kinetically facile.

Introduction

Over the past decade, groundbreaking studies on unnatural biocatalysis have transformed the biochemical landscape of natural enzymes to encompass biocatalytic reactions that were never previously encountered in nature[1-5]. Recently, biocatalysis researchers have discovered a range of useful unnatural enzymatic activities, particularly asymmetric free radical transformations with metalloenzymes[6-10] as well as nicotinamide-[11,12], flavin-[11,12], and pyridoxal phosphate (PLP)[13]-dependent enzymes. Together, these efforts substantially expanded the reaction territory of enzyme catalysis and furnished powerful tools for asymmetric synthesis. Despite these notable advances,

new-to-nature enzymatic C–F bond formation has long eluded the biocatalysis community. The dearth of fluorination enzymatic functions is in stark contrast to the ubiquity of organofluorine compounds in the pharmaceutical and agrochemical industries, as the incorporation of fluorine into organic compounds can often lead to improved bioavailability, enhanced metabolic stability, and desirable protein binding affinity[14-17]. In light of the broad utility of organofluorine compounds, particularly those possessing a fluorinated stereogenic centre[18], fluorine biocatalysis[19] and fluorine synthetic biology[20-23] have long captivated synthetic chemists and synthetic biologists. Among the various fluorination methods[24,25], biocatalytic enantioselective C(sp^3)–H fluorination would be particularly valuable[10], as only a handful of chemocatalytic asymmetric C(sp^3)–H fluorination methods are available to non-enolate systems[26,27], further highlighting the challenge in imposing stereocontrol over fluorination processes. Among these, highly enantioselective C(sp^3)–H fluorination using a free radical mechanism[26] is particularly challenging. The successful implementation of stereoselective biocatalytic fluorination will provide a more sustainable alternative to traditional resource-intensive chemical syntheses of fluorinated medicinal agents[28,29].

To date, fluorinases discovered from bacteria and archaea represent the only natural enzyme class capable of incorporating a fluorine atom to organic substrates (**Fig. 1a**).[30] Using a simple bimolecular nucleophilic substitution (S_N2) mechanism, natural fluorinases catalyse the conversion of *S*-adenosylmethionine (SAM) to 5'-fluoro-5'-deoxyadenosine (5'-FDA), giving rise to fluorometabolites through downstream biosynthetic pathways.[20,30] On the other hand, an array of α-ketoglutarate (αKG)-dependent nonheme Fe enzymes has been discovered and engineered to facilitate C–H (pseudo)halogenation reactions[31-34], including chlorination[33-35], bromination[36], azidation[37-39] and nitration[37] (**Fig. 1b**). Mechanistically, these nonheme Fe enzymes generate a carbon-centred radical by hydrogen atom transfer (HAT) via the intermediacy of (X)Fe(IV)=O (X = (pseudo)halide). The incipient carbon-centred radical subsequently undergoes halogen atom transfer with the Fe(III)–X intermediate, leading to C–H halogenated products[31-34]. Despite extensive studies, to date, converting nonheme Fe halogenases to fluorinases has not been met with success. Several mechanistic rationales, including the low binding affinity of Fe enzymes toward the aqueous fluoride ion (F^-) owing to the high hydration energy of F^- [40], challenging formation of the ferryl intermediate from the putative Fe(II)–F species, and difficulties steering the radical rebound activity toward the Fe(III)–F over Fe(III)–OH moiety, have been postulated to account for this long-standing challenge.

To address these limitations, we capitalised on a new-to-nature enzymatic mechanism to discover and evolve Fe enzymes for asymmetric C–F bond formation. In 2021, our group implemented metalloredox radical biocatalysis as a general means to develop unnatural biocatalytic radical reactions (**Fig. 1c**)[6-8]. In our prior study, we engineered P450 enzymes as atom transfer radical cyclases to catalyse stereocontrolled bromine atom transfer[6,7]. Contemporaneous to our studies, elegant work from the Huang laboratory led to highly efficient nonheme Fe azidases using a radical relay strategy[9]. Parallel to the study from the Huang group, we independently posited that if we could concurrently generate a transient carbon-centred radical and a Fe(III)–F intermediate through a metalloredox atom transfer mechanism (**Figs. 1c** and **1d**), we would be able to bypass the energetically demanding fluoride binding step as well as the ferryl intermediate formation for radical generation, thus directly interrogating the feasibility of C–F bond formation with Fe-dependent enzymes. Specifically, inspired by non-stereoselective small-molecule Fe catalysis[41,42], our proposal for the biocatalytic asymmetric fluorination using Fe enzymes is outlined in **Fig. 1d**. Starting from the *N*-fluoroamide (**I**), fluorine atom transfer to the Fe(II) enzyme (**II**) would lead to a nitrogen-centred radical (*i.e.*, amidyl radical **III**) and an Fe(III)–F species (**IV**).

Due to the high N–H bond dissociation enthalpy (BDE (N–H) = 103.7 kcal·mol^{-1} as determined by our DFT calculations (see the Supplementary **Fig. S16** for details), rapid 1,5-hydrogen atom transfer (1,5-HAT) of **III** would lead to a new carbon-centred radical (**V**). At this stage, stereoselective radical rebound of **V** with the enzymatic Fe(III)–F intermediate **IV** would lead to C–F bond formation **VI** and convert the ferric enzyme to its ferrous state, thereby completing the catalytic cycle. If successfully implemented, this work would lead to the first examples of metalloenzymes capable of forming C–F bonds. Furthermore, it would provide a rare example of highly enantioselective C(sp^3)–H fluorination using an open-shell mechanism.

Results and discussion

Discovery of C–H fluorinating enzyme activities

We commenced our investigation by evaluating an in-house collection of ca. 200 metalloproteins and their variants, including diverse heme and nonheme Fe proteins, by high throughput experimentation using 24- or 96-well plates. All the identified active biocatalysts were then validated, and representative results are summarized in **Fig. 2a**. Among all the heme proteins we evaluated, only reduced amide **3a** derived from the *N*-fluoroamide substrate **1a** was observed in varying yields (Table S1). For example, our previously evolved P450 atom transfer radical cyclases P450$_{ATRCase1}$ possessing a Fe-binding serine residue (Table S1, entry 1) and P450$_{ATRCase2}$ lacking an Fe-binding residue (Table S1, entry 2)[6] provided **3a** in 14% and 17% yield, respectively, with no measurable **2a** formation. In contrast to heme proteins, a set of fluorination biocatalysts emerged from the nonheme Fe enzyme superfamily. Among these, isopenicillin N synthase (IPNS) from *Emericella nidulans* with a two-histidine-one-carboxylate facial triad[43] provided the desired C–H fluorination product **2a** in 0.2% yield and 10:90 enantiomeric ratio (e.r.) (**Fig. 2a**, see **Tables S1** and **S2** for further details). Anthocyanidin synthase from *Arabidopsis thaliana*[44] furnished **2a** in 0.4% yield and 37:63 e.r.. Additionally, quercetin 2,3-dioxygenase from *Bacillus subtilis* (*Bsu*QueD) with a three-histidine-one-carboxylate coordination sphere[45] also afforded **1a** in 0.2% yield and 29:71 e.r.. Furthermore, 1-aminocyclopropane-1-carboxylic acid oxidase (ACCO) from *Petunia hybrida*[46,47], a plant-derived nonheme Fe enzyme with a two-histidine-one carboxylate facial triad whose native function is to produce ethylene from 1-aminocyclopropane-1-carboxylic acid[46], furnished fluorinated **2a** in 0.9% yield and 10:90 e.r.. Finally, natural Fe- and αKG-dependent C–H halogenases, including SyrB2 (Table S1, entry 7),[48,49] WelO5 (Table S1, entry 8),[35,50-55] and BesD (Table S1, entry 9),[56-58] were found to be ineffective in facilitating this unnatural C(sp^3)–H fluorination.

Directed evolution of C–H fluorinating enzyme ACCO$_{CHF}$

Due to the high levels of enantioselectivity and slightly better initial activity observed with wild-type (wt) *P. hybrida* ACCO, we selected this nonheme Fe enzyme as the template for the further development of an efficient C(sp^3)–H fluorinating biocatalyst (**Fig. 2b**). Guided by the crystal structure of ACCO and our molecular docking studies, we first performed site-saturation mutagenesis (SSM) and screening by targeting amino acid residues in proximity to the nonheme Fe centre. Surprisingly, only a single beneficial mutation I184A with modest activity improvement was found among residues in the closest sphere of Fe (**Fig. 2b**, entry 2 and **Table S3**). In light of the relatively small size of ACCO's native substrate 1-aminocyclopropane-1-carboxylic acid (see the SI for further details), we postulated that substrate tunnel engineering might be required for this nonheme enzyme to better accommodate bulky non-native substrates. We thus turned our attention to amino acid residues in the β-sheets of the substrate tunnel in protein engineering. In

each round of engineering, we selected four tunnel residues for SSM. The best performing variant from the four SSM libraries was then selected as the basis for further optimisation. Through iterative saturation mutagenesis (ISM) and screening, five beneficial mutations distal to the Fe centre were identified in the tunnel-defining β-sheets. Among these, residue 158 was found to play a critical role in modulating the fluorination activity and enantioselectivity. While the incorporation of K158N into ACCO I184A resulted in 1.4-fold higher yield and similar enantioselectivity (**Fig. 2b**, entry 3, (2.3 ± 0.1)% yield, 19:81 e.r.), the K158I variant of ACCO I184A furnished **2a** with 3.2-fold higher yield and inverted enantiopreference (entry 4, (4.5 ± 0.2)% yield, 74:26 e.r.). The inverted stereochemistry observed with ACCO I184A K158I relative to that with ACCO I184A is surprising, as the α-carbon of K158 is 10.8 Å away from the Fe centre. These results demonstrated that remote residues such as 158 could influence not only the activity but also the enantioselectivity of ACCO in the current unnatural C–H fluorination.

In further directed evolution, F91L was found to be another key mutation providing 6.6-times higher yield and improved enantioselectivity of **2a** (entry 5, (29.5 ± 0.5)% yield and 84:16 e.r.). Notably, ACCO I184A K158I F91L was the first variant in this evolutionary lineage favouring the formation of C–H fluorination over the undesired reduction (**2a**:**3a** = 82:18), giving rise to substantially enhanced chemoselectivity. Ultimately, after an additional three rounds of SSM and screening (entries 6–8), directed evolution led to ACCO I184A K158I F91L K172Y K93Q T89A ($ACCO_{CHF}$, CHF = C–H fluorination), furnishing the enantioenriched fluorination product **2a** in (97 ± 2)% yield, 95:5 e.r., 98:2 chemoselectivity and (211 ± 5) total turnover number (TTN, entry 8). By further lowering the biocatalyst loading via decreasing the optical density of *E. coli* cells (OD_{600} = 10) overexpressing $ACCO_{CHF}$, a TTN of (601 ± 5) could be achieved without lowering the yield of **2a** (entry 9). Further decreasing OD_{600} to 5 led to a TTN of (820 ± 10). Importantly, among all the nonheme Fe enzymes we investigated, $ACCO_{CHF}$ represents the only biocatalyst capable of delivering enantioenriched fluorinated products in excellent yields without forming other side products, such as the reduction products and C–H hydroxylation products. Furthermore, 550 mg of evolved $ACCO_{CHF}$ could be obtained from 1L *E. coli* culture in TB, which represented a 1.7-fold improvement in protein expression level relative to wt ACCO and underscored its utility in preparative biotransformations (**Table S15** and **Fig. S12**).

We further characterized the Michaelis–Menten kinetics of two intermediate variants ACCO I184A K158I F91L K172Y, ACCO I184A K158I F91L K172Y K93Q and the final variant $ACCO_{CHF}$ using purified enzymes in the presence of stoichiometric quantities of dithionite as the reductant (**Figs. S6–S8**). Michaelis–Menten kinetics showed that while the k_{cat} value of these ACCO variants remained approximately unchanged (2.1 min^{-1}, 2.5 min^{-1} and 2.3 min^{-1}, respectively), the K_M value of this evolutionary series decreased from 520 μM to 420 μM to 210 μM. Together, the k_{cat}/K_M value of these variants increased from 4.0 $mM^{-1}min^{-1}$ to 6.0 $mM^{-1}min^{-1}$ to 11 $mM^{-1}min^{-1}$. Thus, these results indicated that the improved enzymatic activity towards C–H fluorination originated from enhanced substrate binding, which may arise from substrate tunnel engineering.

Substrate scope of biocatalytic asymmetric C–H fluorination

With the evolved variant $ACCO_{CHF}$ in hand, we next examined the substrate scope of this biocatalytic enantioselective C(sp^3)–H fluorination. Substituents at the 3, 4, and 5 positions of the aromatic ring were compatible, providing the corresponding fluorinated products in good to excellent enantioselectivity (**2b**, **2c**, and **2d**). Electron-withdrawing fluorine (**2e**) and chlorine (**2f**)

substituents as well as electron-donating methoxy (**2g**) were compatible with this transformation. *Tert*-Amyl amides (**2h**) could also be transformed with good enantioselectivity. Furthermore, extended aliphatic substituents, including a propyl (**2i**), a homoallyl (**2j**) and a methoxyethyl (**2k**) group, could be efficiently fluorinated with excellent enantiocontrol. A tetrahydronaphthalene core (**2l**) also underwent biotransformation to furnish the corresponding enantioenriched fluorinated product. Additionally, tertiary C(sp^3)–H bonds could also be efficiently and chemoselectively fluorinated to provide the desired fluorination product (**2i**) in excellent yields. A thiophene containing substrate **1n** could also undergo C–H fluorination with excellent enantioselectivity and chemoselectivity (90:10 e.r., **2n**:**3n** = 88:12, see the SI for details). Additional examples of unsuccessful substrates are provided in the SI. For example, primary C(sp^3)–H bonds (**1o**) could not be efficiently fluorinated with evolved $ACCO_{CHF}$. *N*-fluoroacrylamide **1p** was transformed with low activity but excellent enantio- and chemoselectivity.

Importantly, the excellent catalytic activity, enantioselectivity, and chemoselectivity of $ACCO_{CHF}$ allowed this biocatalytic C–H fluorination to be easily carried out on a gram-scale with a relatively small amount of whole-cell biocatalysts, demonstrating the practicality of this biotransformation. The absolute stereochemistry of **2a** was ascertained by single crystal X-ray diffraction analysis (see the SI for details).

Mechanistic insights from computational investigations

Our radical clock experiment with a cyclopropyl substrate indicated the formation of cyclopropane ring-opening product, consistent with the proposed radical mechanism (see the SI for details). To gain further insights into the mechanism and the roles of active site residues of this new-to-nature biocatalytic C(sp^3)–H fluorination, we performed computational studies using classical molecular dynamics (MD) simulations and density functional theory (DFT) calculations (see the SI for computational details). First, classical MD simulations of the complexes of *N*-fluoroamide **1a** with both wt ACCO and $ACCO_{CHF}$ variants were carried out to study the preferred substrate binding modes and to identify key active site residues involved in substrate binding (**Fig. 4**). In order to model the substrate near-attack-conformations[59] that promote the fluorine atom transfer step, the Fe–F distance was restrained to be within 3.0–3.2 Å using a harmonic potential of 100 $kcal \cdot mol^{-1} \cdot Å^{-2}$.[9] The restrained MD simulations showed that in order to minimise unfavourable steric repulsions with the protein scaffold, substrate **1a** approaches the Fe centre from the coordination site *trans*- to H234. Furthermore, these MD studies indicated that mutations K158I, F91L, and T89A widen the substrate entrance tunnel, providing more space to facilitate the transport of the bulky *N*-fluoroamide substrate **1a** into the active site. In particular, mutations K158I and F91L greatly reduce the bulkiness of these tunnel bottleneck residues, increasing the tunnel bottleneck radius from 3.12 Å in wt ACCO to 4.17 Å in $ACCO_{CHF}$ (see **Fig. S15**). In addition, the I184A mutation opens up more space to accommodate **1a**, allowing the fluorine atom in **1a** to approach the Fe centre while circumventing unfavourable steric clashes between the adjacent *N*-*t*Bu group of **1a** and active site residues.

Next, to elucidate the reactivities of the unnatural fluorine atom transfer and fluorine rebound steps, we performed DFT calculations of the reaction energy profile of this biocatalytic C–H fluorination. We constructed a truncated model based on the active site geometry of the ACCO enzymes, in which imidazole (Im) and acetate (AcO) groups are used to model aspartate and histidine residues, respectively[60]. Our DFT calculations indicate that all the intermediates and transition states in the catalytic cycle feature a high-spin quintet Fe(II) and sextet Fe(III)[9] centres (see **Fig. S18** for computed energy profile at the less favorable intermediate-spin state). Previous

studies indicated that fluorine atom transfer to a transition metal centre is kinetically more challenging than the analogous chlorine and bromine atom transfer, due to the higher bond dissociation energy (BDE) of the fluorine atom donor. In addition, fluorine atom rebound from a transition metal fluoride is also slower than other halogens because of the strong metal fluoride bond[61]. In contrast, the computed reaction energy profile (**Fig. 5**) reveals a relatively low barrier of 11.8 kcal·mol^{-1} for the initial fluorine atom transfer (**TS-1**). Here, the high exothermicity (−14.3 kcal·mol^{-1}) in converting an activated N–F bond in **4** to a stronger Fe(III)–F bond provides the thermodynamic driving force for substrate activation. In addition, the Fe(II) centre in **4** has a relatively high HOMO energy of −7.03 eV, promoting the charge transfer (0.31 *e*) from the Fe centre to the *N*-fluoroamide substrate **1a** at the transition state (**TS-1**). After the fluorine atom transfer, the nitrogen-centred radical in complex **5** undergoes rapid 1,5-hydrogen atom transfer via **TS-2** to provide the benzyl radical intermediate **6**. Finally, radical rebound with the Fe(III)–F species leading to C–F bond formation via **TS-3** is found to be highly kinetically facile, displaying an activation barrier of 3.4 kcal·mol^{-1} with respect to **6**. Unlike other transition metal fluorides featuring a strong M–F bond with BDEs higher than 100 kcal·mol^{-1}[62], the Fe(III)–F bond in **6** has a weaker BDE of 81.4 kcal·mol^{-1}, allowing thermodynamically downhill fluorine rebound to form the benzylic C–F bond with a BDE of 98.1 kcal·mol^{-1}. In addition, the heterolytic dissociation of F^- from Fe(III)–F in **5** and **6** was found to be thermodynamically unfavourable (**Fig. S19**), allowing for productive C–F bond formation via the radical rebound pathway. We note that the low activation energy required for C–F bond formation involving an enzymatic Fe(III)–F intermediate has broad implications in repurposing natural nonheme Fe halogenases as fluorinases.

Conclusion

In summary, we repurposed and evolved a nonheme Fe enzyme 1-aminocyclopropane-1-carboxylic acid oxidase (ACCO) to catalyse C(sp^3)–H fluorination reactions with excellent levels of chemo- and enantiocontrol. Our evolved Fe-dependent enzyme ACCO$_{CHF}$ constitutes the first new-to-nature C–F bond forming biocatalyst, which has long been sought after in biocatalysis, synthetic biology, and bioinorganic chemistry. By exploiting an underutilised radical mechanism for enzymatic C–F bond formation, the current new-to-nature fluorinating enzymes complement the only naturally occurring fluorinase relying on a closed-shell S_N2 mechanism for fluorination. Furthermore, this biocatalytic fluorination represents a rare method for catalytic asymmetric C(sp^3)–H fluorination and the only radical C–H fluorination with excellent enantiocontrol. The utility of our newly evolved nonheme enzymes was further demonstrated in the gram-scale preparation of enantioenriched organofluorides. Together, the evolution of efficient and selective Fe-dependent fluorinating enzymes affords a valuable tool for the biological synthesis of chiral organofluorine compounds via a C–H functionalization logic, thereby setting the stage for the further advancement of fluorine biocatalysis and synthetic biology.

Methods

Expression of ACCO$_{CHF}$ variants.

E. coli BL21(DE3) cells harbouring recombinant plasmid encoding the appropriate ACCO variant were grown overnight at 37 °C and 230 rpm in 4 mL LB media supplemented with 0.05 mg/mL kanamycin (LB$_{kan}$). Preculture (1.5 mL, 5% v/v) was used to inoculate 28.5 mL TB media supplemented with 0.05 mg/mL kanamycin (TB$_{kan}$) in a 125 mL Erlenmeyer flask. The culture was incubated at 37 °C and 230 rpm for 2 h to reach an OD_{600} of approximately 1.5. The culture was then cooled on ice for 20 min and induced with 0.5 mM isopropyl β-D-1-thiogalactopyranoside

(IPTG, final concentrations). Protein expression was performed at 20 °C and 200 rpm for 20 h. The cells were then transferred to a conical tube (50 mL) and harvested by centrifugation (3434 *g*, 4 min, 4 °C) using an Eppendorf 5910R tabletop centrifuge.

Analytical scale enantioselective biocatalytic C–H fluorination. The suspension of *E. coli* cells expressing ACCO in M9-N buffer (typically OD_{600} = 10–30, 540 µL) was added to a vial (2 mL) and kept on ice. This vial was then transferred into an anaerobic chamber, where the solution of Mohr's salt (30 µL, 13.3 mM stock solution in degassed H_2O) and the *N*-fluoroamide substrate (30 µL, 133 mM stock solution in MeCN) was added. The final reaction volume was 600 µL; the final concentration of the *N*-fluoroamide substrate was 6.67 mM. (Note: the reaction performed with *E. coli* cells resuspended to OD_{600} = 30 indicates that 540 µL cell suspension with an OD_{600} of 30 were added.) The vials were sealed and shaken on a Corning digital microplate shaker at room temperature and 680 rpm for 24 h. The reaction mixture was then analyzed by chiral HPLC.

Gram scale enantioselective biocatalytic C–H fluorination. *E. coli* BL21(DE3) cells harbouring the recombinant plasmid encoding $ACCO_{CHF}$ were grown overnight at 37 °C and 230 rpm in 25 mL LB media supplemented with 0.05 mg/mL kanamycin (LB_{kan}). Preculture (20 mL, 2% v/v) was used to inoculate 1 L TB media supplemented with 0.05 mg/mL kanamycin (TB_{kan}) in a 4 L Erlenmeyer flask. The culture was incubated at 37 °C and 230 rpm for 2.5 h to reach an OD_{600} of approximately 1.5. The culture was then cooled on ice for 30 min and induced with 0.5 mM isopropyl β-D-1-thiogalactopyranoside (IPTG, final concentrations). Protein expression was performed at 20 °C and 200 rpm for 20 h.

The cells were harvested by centrifugation (3214 *g*, 5 min, 4 °C) using a Thermo Scientific Sorvall Lynx 6000 superspeed centrifuge and resuspended in M9-N buffer (OD_{600} = 30). An aliquot of *E. coli* cell suspension (2 mL) was taken to determine protein concentration using the SDS-PAGE assay. Cell suspensions in M9-N buffer were kept on ice until use. (Note: leaving the cell suspension at room temperature for an extended period of time will lead to significantly reduced enzyme activity.) To a 1 L Erlenmeyer flask equipped with a screw cap was added a suspension of *E. coli* cells in M9-N buffer expressing the desired enzyme variant. The flask was transferred to an anaerobic chamber, where a solution of Mohr's salt (5 mL, 150 mM stock solution in degassed H_2O) and the *N*-fluoroamide substrate (1.67 g, 7.5 mmol, 500 mM in MeCN, 15 mL for substrate **1a**) were added. The flask was capped, sealed with parafilm, taken out of the anaerobic chamber and allowed to shake in an Eppendorf Innova 44R shaker at room temperature and 230 rpm for 24 h.

Upon the completion of this biotransformation, the reaction mixture was extracted with 300 mL EtOAc. The mixture was transferred to a 1 L ultracentrifugation bucket and spun down (4629 *g*, 10 min) using a Thermo Scientific Sorvall Lynx 6000 superspeed centrifuge to separate the organic layer from the aqueous layer. The aqueous layer was extracted with EtOAc for an additional five times. Combined organic layers were dried over $MgSO_4$ and an aliquot of the organic layer (400 µL) was used for product enantioselectivity via chiral HPLC. Combined organic layers were concentrated *in vacuo* with the aid of a rotary evaporator and purified by column chromatography with the aid of a Biotage Isolera to afford the desired organofluoride product **2a** in 88% yield and 95:5 e.r..

Acknowledgements

This research is supported by the NIH (R35GM147387 to Y.Y.), NSF (CHE-2247505 to P.L.) and Boehringer Ingelheim's IU More Green Grant (BI # 763955 to Y.Y.). We acknowledge the NSF

BioPACIFIC MIP (DMR-1933487) and NSF MRSEC at UCSB (DMR-2308708) for access to instrumentation. Computational studies were carried out at the University of Pittsburgh Center for Research Computing and the Advanced Cyberinfrastructure Coordination Ecosystem: Services & Support (ACCESS) program, supported by NSF award numbers OAC-2117681, OAC-1928147 and OAC-1928224. We thank Prof. Yiming Wang (University of Pittsburgh) for critical reading of this manuscript.

Data availability: All data are available in the main text and the Supplementary Information. Plasmids encoding evolved ACCO variants reported in this study are available for research purposes from Y.Y. under a material transfer agreement with the University of California Santa Barbara. Solid-state structure of **2a** is available free of charge from the Cambridge Crystallographic Data Centre under reference number CCDC 2294341. All the protein structures used are available from the protein data bank using their accession numbers.

Author contributions

Y.Y. conceived and directed the project. L.Z. performed all the enzyme engineering, Michaelis–Menten kinetics, substrate synthesis, and substrate scope studies. Y.Y., L.C. and Y.-L.Z. performed enzyme mining. L.Z. and L.C. performed initial enzyme evaluation. F.G. and R.G. provided some substrates. B.K.M. carried out the computational studies with P.L. providing guidance. H.W. and Y.-D.Z. participated in discussions and provided suggestions. Y.Y., L.Z., P.L. and B.K.M. wrote the manuscript with the input of all other authors.

Competing interests

The authors declare no competing interests.

Fig. 1. Enzymatic fluorination: an overview. a, The only known fluorinating enzyme: naturally occurring fluorinase that catalyses the conversion of *S*-adenosylmethionine (SAM) to 5'-fluorodeoxyadenosine (5'-FDA)[30]. **b,** Naturally occurring nonheme Fe C(sp^3)–H halogenases that catalyse the conversion of C–H bonds to C–X bonds (X = Cl, Br, N_3 and NO_2)[31-34]. **c,** Our previously evolved unnatural heme-dependent atom transfer halogenases[6-8]. **d,** This work: evolved nonheme Fe enzymes for unnatural enantioselective C(sp^3)–H fluorination. Enzyme images were generated using PyMOL from PDB structures 4H23 and 1W9Y. S_N2 = bimolecular nucleophilic substitution, His = histidine, Asp = aspartate, HAT = hydrogen atom transfer, XAT = halogen atom transfer.

Fig. 2. Development of chemo- and enantioselective nonheme Fe enzyme $ACCO_{CHF}$ for new-to-nature C(sp^3)–H fluorination: enzyme mining and engineering. a, Discovery of fluorine atom transfer activity among Fe-dependent enzymes. **b,** Directed evolution of $ACCO_{CHF}$ as a highly chemo- and enantioselective C–H fluorinating enzyme. Active-site illustration of ACCO was made using Pymol from PDB ID: 1W9Y. ACCO = 1-aminocyclopropane-1-carboxylic acid oxidase, His = histidine, Asp = aspartate, e.r. = enantiomeric ratio, TTN = total turnover number. OD_{600} = optical density of *E. coli* cells measured at 600 nm in 1 cm light path.

Fig. 3. Substrate scope of $ACCO_{CHF}$-catalysed asymmetric C(sp^3)–H fluorination. Reaction conditions: suspensions of *E. coli* cells harbouring $ACCO_{CHF}$ (540 μL in M9-N), $(NH_4)_2Fe(SO_4)_2$

(30 μL, 13.3 mM in degassed H_2O) and *N*-fluoroamide substrate **1** (30 μL, 133 mM in MeCN), 680 rpm, 24 h. [a]1.5-gram scale synthesis was carried out using whole *E. coli* cells derived from 1 L of TB expression culture. See the Supplementary Information for details. r.t., room temperature; CCO = 1-aminocyclopropane-1-carboxylic acid oxidase.

Fig. 4. The Most populated structures of the enzyme–substrate complexes from MD simulations. a, The most populated structures from restrained MD simulations of the enzyme–substrate complexes of **1a** with wt ACCO. **b,** The most populated structures from restrained MD simulations of the enzyme–substrate complexes of **1a** with $tACCO_{CHF}$ variants. Substrate entrance tunnels are shown in orange. MD = molecular dynamics, ACCO = 1-aminocyclopropane-1-carboxylic acid oxidase.

Fig. 5. Computational studies using a truncated active site model. a, DFT-computed reaction energy profile of C–H fluorination of *N*-fluoroamide **1** using a truncated model based on the active site of ACCO enzyme at the (U)B3LYP-D3(BJ)/def2-TZVP/SMD//(U)B3LYP-D3(BJ)/6-31G(d)–SDD(Fe) level of theory. Energies are with respect to **4**. Imidazole (Im) and acetate (AcO) groups are models for aspartate and histidine residues, respectively. **b,** Optimized geometries of the fluorine atom transfer (**TS-1**) and fluorine radical rebound (**TS-3**) transition states. Ac, acetyl; Im, imidazole

References

1 Renata, H., Wang, Z. J. & Arnold, F. H. Expanding the Enzyme Universe: Accessing Non-Natural Reactions by Mechanism-Guided Directed Evolution. *Angew. Chem. Int. Ed.* **54**, 3351-3367 (2015).

2 Brandenberg, O. F., Fasan, R. & Arnold, F. H. Exploiting and engineering hemoproteins for abiological carbene and nitrene transfer reactions. *Curr. Opin. Biotechnol.* **47**, 102-111 (2017).

3 Leveson-Gower, R. B., Mayer, C. & Roelfes, G. The importance of catalytic promiscuity for enzyme design and evolution. *Nat. Rev. Chem.* **3**, 687-705 (2019).

4 Chen, K. & Arnold, F. H. Engineering new catalytic activities in enzymes. *Nat. Catal.* **3**, 203-213 (2020).

5 Klaus, C. & Hammer, S. C. New catalytic reactions by enzyme engineering. *Trends Chem.* **4**, 363-366 (2022).

6 Zhou, Q., Chin, M., Fu, Y., Liu, P. & Yang, Y. Stereodivergent atom-transfer radical cyclization by engineered cytochromes P450. *Science* **374**, 1612-1616 (2021).

7 Fu, Y. *et al.* Engineered P450 Atom-Transfer Radical Cyclases are Bifunctional Biocatalysts: Reaction Mechanism and Origin of Enantioselectivity. *J. Am. Chem. Soc.* **144**, 13344-13355 (2022).

8 Fu, W. *et al.* Enzyme-controlled stereoselective radical cyclization to arenes enabled by metalloredox biocatalysis. *Nat. Catal.* **6**, 628-636 (2023).

9 Rui, J. *et al.* Directed evolution of nonheme iron enzymes to access abiological radical-relay $C(sp^3)$−H azidation. *Science* **376**, 869-874 (2022).

10 Ren, X. & Fasan, R. Engineered and artificial metalloenzymes for selective C–H functionalization. *Curr. Opin. Green Sustain. Chem.* **31**, 100494 (2021).

11 Emmanuel, M. A. *et al.* Photobiocatalytic Strategies for Organic Synthesis. *Chem. Rev.* **123**, 5459-5520 (2023).
12 Harrison, W., Huang, X. & Zhao, H. Photobiocatalysis for Abiological Transformations. *Acc. Chem. Res.* **55**, 1087-1096 (2022).
13 Cheng, L. *et al.* Stereoselective amino acid synthesis by synergistic photoredox-pyridoxal radical biocatalysis. *Science* **381**, 444-451 (2023).
14 Wang, J. *et al.* Fluorine in Pharmaceutical Industry: Fluorine-Containing Drugs Introduced to the Market in the Last Decade (2001–2011). *Chem. Rev.* **114**, 2432-2506 (2014).
15 Gillis, E. P., Eastman, K. J., Hill, M. D., Donnelly, D. J. & Meanwell, N. A. Applications of Fluorine in Medicinal Chemistry. *J. Med. Chem.* **58**, 8315-8359 (2015).
16 Zhou, Y. *et al.* Next Generation of Fluorine-Containing Pharmaceuticals, Compounds Currently in Phase II–III Clinical Trials of Major Pharmaceutical Companies: New Structural Trends and Therapeutic Areas. *Chem. Rev.* **116**, 422-518 (2016).
17 Ogawa, Y., Tokunaga, E., Kobayashi, O., Hirai, K. & Shibata, N. Current Contributions of Organofluorine Compounds to the Agrochemical Industry. *iScience* **23**, 101467 (2020).
18 Inoue, M., Sumii, Y. & Shibata, N. Contribution of Organofluorine Compounds to Pharmaceuticals. *ACS Omega* **5**, 10633-10640 (2020).
19 Wu, L., Maglangit, F. & Deng, H. Fluorine biocatalysis. *Curr. Opin. Chem. Biol.* **55**, 119-126 (2020).
20 Walker, M. C. & Chang, M. C. Y. Natural and engineered biosynthesis of fluorinated natural products. *Chem. Soc. Rev.* **43**, 6527-6536 (2014).
21 Walker, M., C. *et al.* Expanding the Fluorine Chemistry of Living Systems Using Engineered Polyketide Synthase Pathways. *Science* **341**, 1089-1094 (2013).
22 Sirirungruang, S. *et al.* Engineering site-selective incorporation of fluorine into polyketides. *Nat. Chem. Biol.* **18**, 886-893 (2022).
23 Rittner, A. *et al.* Chemoenzymatic synthesis of fluorinated polyketides. *Nat. Chem.* **14**, 1000-1006 (2022).
24 Szpera, R., Moseley, D. F. J., Smith, L. B., Sterling, A. J. & Gouverneur, V. The Fluorination of C−H Bonds: Developments and Perspectives. *Angew. Chem. Int. Ed.* **58**, 14824-14848 (2019).
25 Leibler, I. N.-M., Gandhi, S. S., Tekle-Smith, M. A. & Doyle, A. G. Strategies for Nucleophilic C(sp^3)–(Radio)Fluorination. *J. Am. Chem. Soc.* **145**, 9928-9950 (2023).
26 Huang, X. *et al.* Late Stage Benzylic C–H Fluorination with [^{18}F]Fluoride for PET Imaging. *J. Am. Chem. Soc.* **136**, 6842-6845 (2014).
27 Park, H., Verma, P., Hong, K. & Yu, J.-Q. Controlling Pd(iv) reductive elimination pathways enables Pd(II)-catalysed enantioselective C(sp^3)−H fluorination. *Nat. Chem.* **10**, 755-762 (2018).
28 Britton, R. *et al.* Contemporary synthetic strategies in organofluorine chemistry. *Nature Reviews Methods Primers* **1**, 47 (2021).
29 O'Hagan, D. & Young, R. J. Future challenges and opportunities with fluorine in drugs? *Med. Chem. Res.* **32**, 1231-1234 (2023).
30 O'Hagan, D. & Deng, H. Enzymatic Fluorination and Biotechnological Developments of the Fluorinase. *Chem. Rev.* **115**, 634-649 (2015).
31 Vaillancourt, F. H., Yeh, E., Vosburg, D. A., Garneau-Tsodikova, S. & Walsh, C. T. Nature's Inventory of Halogenation Catalysts: Oxidative Strategies Predominate. *Chem. Rev.* **106**, 3364-3378 (2006).

32 Agarwal, V. *et al.* Enzymatic Halogenation and Dehalogenation Reactions: Pervasive and Mechanistically Diverse. *Chem. Rev.* **117**, 5619-5674 (2017).
33 Crowe, C. *et al.* Halogenases: a palette of emerging opportunities for synthetic biology–synthetic chemistry and C–H functionalisation. *Chem. Soc. Rev.* **50**, 9443-9481 (2021).
34 Papadopoulou, A., Meyer, F. & Buller, R. M. Engineering Fe(II)/α-Ketoglutarate-Dependent Halogenases and Desaturases. *Biochemistry* **62**, 229-240 (2023).
35 Hayashi, T. *et al.* Evolved Aliphatic Halogenases Enable Regiocomplementary C−H Functionalization of a Pharmaceutically Relevant Compound. *Angew. Chem. Int. Ed.* **58**, 18535-18539 (2019).
36 Vaillancourt, F. H., Vosburg, D. A. & Walsh, C. T. Dichlorination and Bromination of a Threonyl-S-Carrier Protein by the Non-heme FeII Halogenase SyrB2. *ChemBioChem* **7**, 748-752 (2006).
37 Matthews, M. L. *et al.* Direct nitration and azidation of aliphatic carbons by an iron-dependent halogenase. *Nat. Chem. Biol.* **10**, 209-215 (2014).
38 Gomez, C. A., Mondal, D., Du, Q., Chan, N. & Lewis, J. C. Directed Evolution of an Iron(II)- and α-Ketoglutarate-Dependent Dioxygenase for Site-Selective Azidation of Unactivated Aliphatic C−H Bonds. *Angew. Chem. Int. Ed.* **n/a**, e202301370 (2023).
39 Chan, N. H. *et al.* Non-Native Anionic Ligand Binding and Reactivity in Engineered Variants of the Fe(II)- and α-Ketoglutarate-Dependent Oxygenase, SadA. *Inorg. Chem.* **61**, 14477-14485 (2022).
40 Zhan, C.-G. & Dixon, D. A. Hydration of the Fluoride Anion: Structures and Absolute Hydration Free Energy from First-Principles Electronic Structure Calculations. *J. Phys. Chem. A* **108**, 2020-2029 (2004).
41 Groendyke, B. J., AbuSalim, D. I. & Cook, S. P. Iron-Catalyzed, Fluoroamide-Directed C–H Fluorination. *J. Am. Chem. Soc.* **138**, 12771-12774 (2016).
42 Pinter, E. N., Bingham, J. E., AbuSalim, D. I. & Cook, S. P. N-Directed fluorination of unactivated Csp^3–H bonds. *Chem. Sci.* **11**, 1102-1106 (2020).
43 Ge, W. *et al.* Isopenicillin N Synthase Mediates Thiolate Oxidation to Sulfenate in a Depsipeptide Substrate Analogue: Implications for Oxygen Binding and a Link to Nitrile Hydratase? *J. Am. Chem. Soc.* **130**, 10096-10102 (2008).
44 Wilmouth, R. C. *et al.* Structure and Mechanism of Anthocyanidin Synthase from Arabidopsis thaliana. *Structure* **10**, 93-103 (2002).
45 Gopal, B., Madan, L. L., Betz, S. F. & Kossiakoff, A. A. The Crystal Structure of a Quercetin 2,3-Dioxygenase from Bacillus subtilis Suggests Modulation of Enzyme Activity by a Change in the Metal Ion at the Active Site(s). *Biochemistry* **44**, 193-201 (2005).
46 Zhang, Z., Ren, J.-S., Clifton, I. J. & Schofield, C. J. Crystal Structure and Mechanistic Implications of 1-Aminocyclopropane-1-Carboxylic Acid Oxidase—The Ethylene-Forming Enzyme. *Chem. Biol.* **11**, 1383-1394 (2004).
47 Houben, M. & Van de Poel, B. 1-Aminocyclopropane-1-Carboxylic Acid Oxidase (ACO): The Enzyme That Makes the Plant Hormone Ethylene. *Front. Plant Sci.* **10** (2019).
48 Vaillancourt, F. H., Yin, J. & Walsh, C. T. SyrB2 in syringomycin E biosynthesis is a nonheme Fe^{II} α-ketoglutarate- and O_2-dependent halogenase. *Proc. Natl. Acad. Sci. USA* **102**, 10111-10116 (2005).
49 Blasiak, L. C., Vaillancourt, F. H., Walsh, C. T. & Drennan, C. L. Crystal structure of the non-haem iron halogenase SyrB2 in syringomycin biosynthesis. *Nature* **440**, 368-371 (2006).

50 Mitchell, A. J. *et al.* Structural basis for halogenation by iron- and 2-oxo-glutarate-dependent enzyme WelO5. *Nat. Chem. Biol.* **12**, 636-640 (2016).
51 Liu, X. in *Methods Enzymol.* Vol. 604 (ed Bradley S. Moore) 389-404 (Academic Press, 2018).
52 Voss, M. *et al.* Enzyme Engineering Enables Inversion of Substrate Stereopreference of the Halogenase WelO5*. *ChemCatChem* **14**, e202201115 (2022).
53 Büchler, J. *et al.* Algorithm-aided engineering of aliphatic halogenase WelO5* for the asymmetric late-stage functionalization of soraphens. *Nat. Comm.* **13**, 371 (2022).
54 Duewel, S. *et al.* Directed Evolution of an FeII-Dependent Halogenase for Asymmetric C(sp3)–H Chlorination. *ACS Catal.* **10**, 1272-1277 (2020).
55 Hillwig, M. L. & Liu, X. A new family of iron-dependent halogenases acts on freestanding substrates. *Nat. Chem. Biol.* **10**, 921-923 (2014).
56 Marchand, J. A. *et al.* Discovery of a pathway for terminal-alkyne amino acid biosynthesis. *Nature* **567**, 420-424 (2019).
57 Neugebauer, M. E. *et al.* A family of radical halogenases for the engineering of amino-acid-based products. *Nat. Chem. Biol.* **15**, 1009-1016 (2019).
58 Neugebauer, M. E. *et al.* Reaction pathway engineering converts a radical hydroxylase into a halogenase. *Nat. Chem. Biol.* **18**, 171-179 (2022).
59 Knorrscheidt, A. *et al.* Accessing Chemo- and Regioselective Benzylic and Aromatic Oxidations by Protein Engineering of an Unspecific Peroxygenase. *ACS Catal.* **11**, 7327-7338 (2021).
60 Usharani, D., Janardanan, D. & Shaik, S. Does the TauD enzyme always hydroxylate alkanes, while an analogous synthetic non-heme reagent always desaturates them? *J. Am. Chem. Soc.* **133**, 176-179 (2011).
61 Lanzalaco, S. *et al.* Atom Transfer Radical Polymerization with Different Halides (F, Cl, Br, and I): Is the Process "Living" in the Presence of Fluorinated Initiators? *Macromolecules* **50**, 192-202 (2017).
62 Aoto, Y. A., de Lima Batista, A. P., Kohn, A. & de Oliveira-Filho, A. G. S. How To Arrive at Accurate Benchmark Values for Transition Metal Compounds: Computation or Experiment? *J Chem Theory Comput* **13**, 5291-5316 (2017).

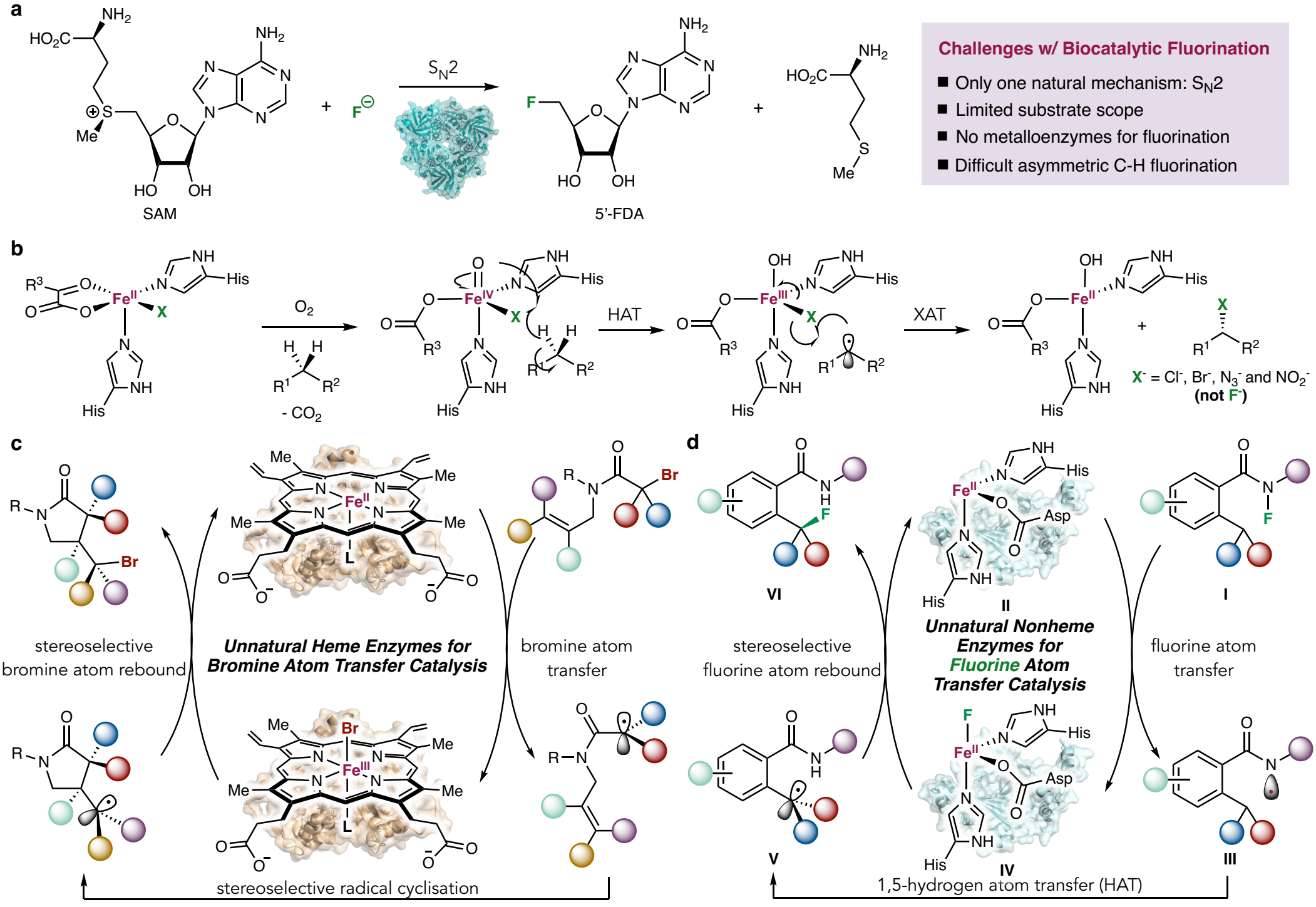
a
SAM
S_N2
5'-FDA
Challenges w/ Biocatalytic Fluorination
Only one natural mechanism: S_N2
Limited substrate scope
No metalloenzymes for fluorination
Difficult asymmetric C-H fluorination
b
O_2
- CO_2
HAT
XAT
X^- = Cl^-, Br^-, N_3^- and NO_2^-
(not F^-)
c
stereoselective
bromine atom rebound
Unnatural Heme Enzymes for
Bromine Atom Transfer Catalysis
bromine atom
transfer
stereoselective radical cyclisation
d
stereoselective
fluorine atom rebound
Unnatural Nonheme
Enzymes for
Fluorine Atom
Transfer Catalysis
fluorine atom
transfer
1,5-hydrogen atom transfer (HAT)
I
II
III
IV
V
VI

a

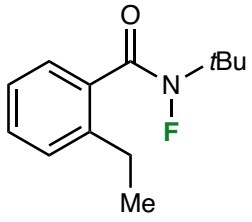

1a

whole *E. coli* cells harboring Fe enzymes

M9-N buffer (pH = 7.4)

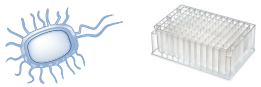

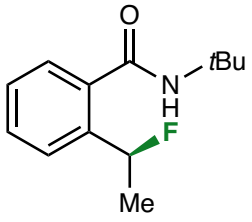

2a

+

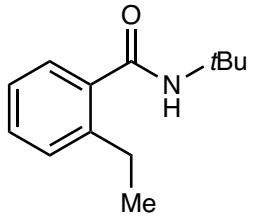

3a

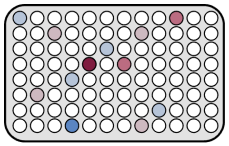

high-throughput experimentation

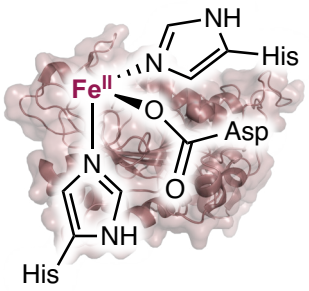

IPNS

0.2% **2a** (10:90 e.r.)

6% **3a**

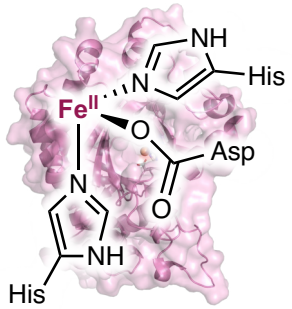

ANS

0.4% **2a** (37:63 e.r.)

11% **3a**

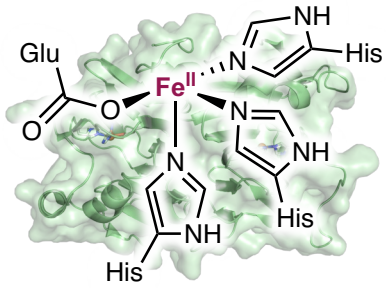

QueD

0.2% **2a** (29:71 e.r.)

17% **3a**

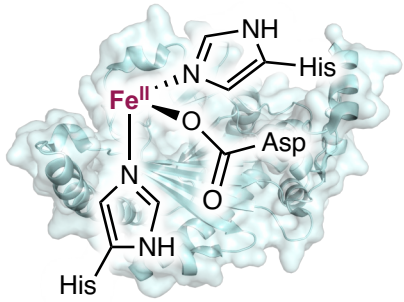

ACCO

0.9% **2a** (10:90 e.r.)

6% **3a**

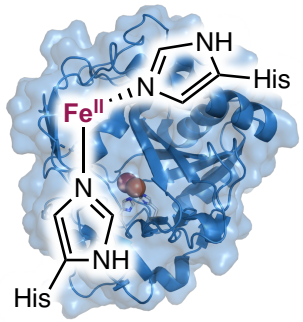

SyrB2

0% **2a**

6% **3a**

b

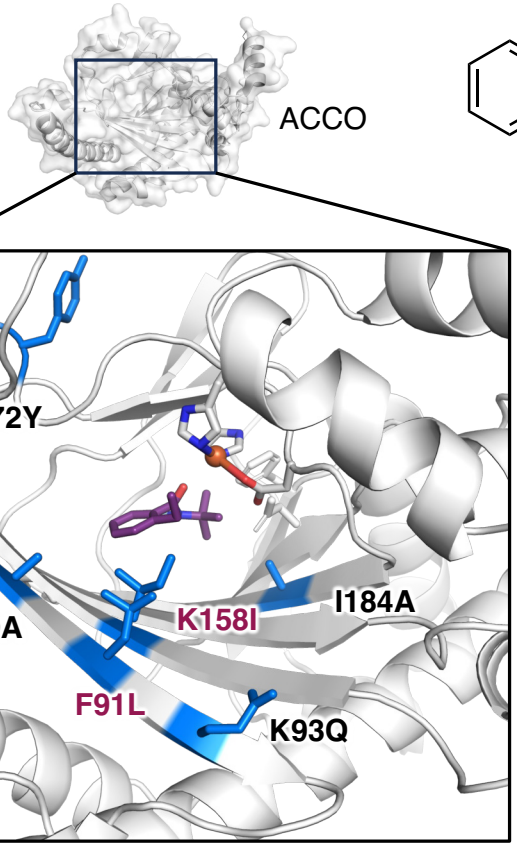

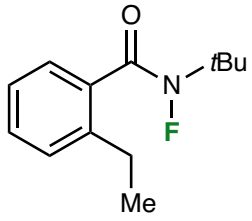

1a

whole *E. coli* cells harboring ACCO variants

$(NH_4)_2Fe(SO_4)_2$

M9-N buffer (pH = 7.4)

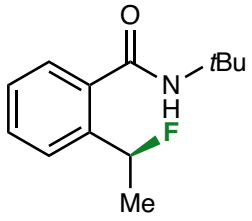

2a

+

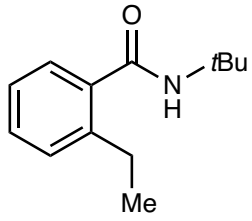

3a

entry	ACCO variant	yield (e.r.) of 2a	TTN	yield of 3a	2a:3a
1	wt ACCO	(0.9 ± 0.1)% (10:90)	3	(5.9 ± 0.1)%	17:83
2	ACCO I184A	(1.4 ± 0.1)% (12:88)	5	(5.6 ± 0.5)%	23:77
3	ACCO I184A K158N	(2.3 ± 0.1)% (19:81)	8	(6.0 ± 0.1)%	29:71
4	ACCO I184A **K158I**	(4.5 ± 0.2)% (**74:26**)	21 ± 1	(5.7 ± 0.3)%	44:56
5	ACCO I184A K158I **F91L**	**(29.5 ± 0.5)% (84:16)**	73 ± 3	(6.6 ± 0.2)%	**82:18**
6	ACCO I184A K158I F91L K172Y	(37.3 ± 0.8)% (88:12)	140 ± 3	(6.4 ± 0.4)%	85:15
7	ACCO I184A K158I F91L K172Y K93Q T89A ($ACCO_{CHF}$)	(76 ± 2)% (92:8)	266 ± 7	(2.8 ± 0.4)%	96:4
8	ACCO I184A K158I F91L K172Y K93Q T89A ($ACCO_{CHF}$)	**(97 ± 2)% (95:5)**	211 ± 5	(1.4 ± 0.1)%	**98:2**
9	$ACCO_{CHF}$ (OD_{600} = 10)	(92 ± 2)% (95:5)	**601 ± 5**	(1.7 ± 0.1)%	98:2
10	$ACCO_{CHF}$ (OD_{600} = 5)	(63 ± 1)% (95:5)	820 ± 10	(1.1 ± 0.1)%	98:2

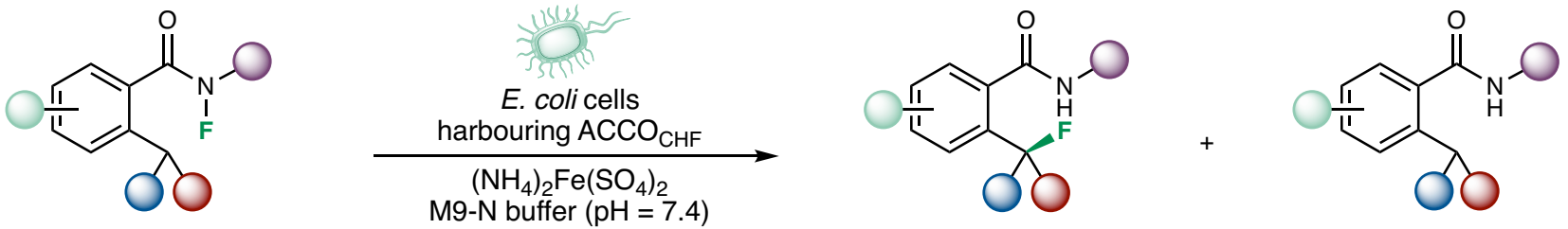

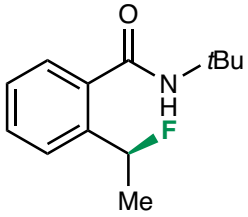

2a
(601 ± 5) TTN
92% yield, 95:5 e.r.
2a:**3a** = 98:2

≡

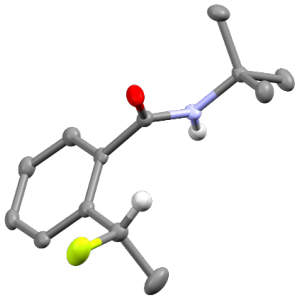

X-ray crystal
structure of **2a**

≡

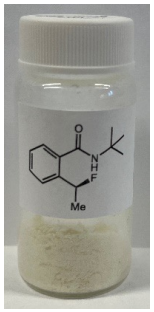

584 TTN
88% yield, 95:5 e.r.
[1.5 gram scale][a]

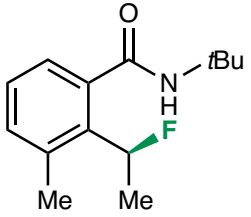

2b
(326 ± 4) TTN
95% yield, 94:6 e.r.
2b:**3b** = 95:5

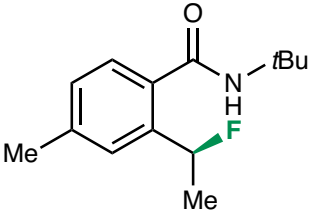

2c
(125 ± 1) TTN
73% yield, 85:15 e.r.
2c:**3c** = 91:9

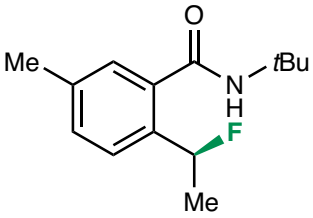

2d
(71 ± 1) TTN
62% yield, 72:28 e.r.
2d:**3d** = 91:9

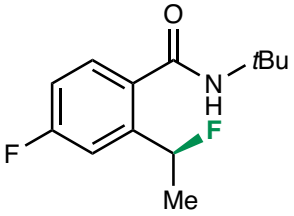

2e
(272 ± 4) TTN
83% yield, 97:3 e.r.
2e:**3e** = 96:4

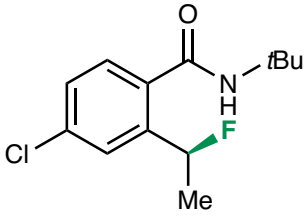

2f
(62 ± 1) TTN
54% yield, 93:7 e.r.
2f:**3f** = 83:17

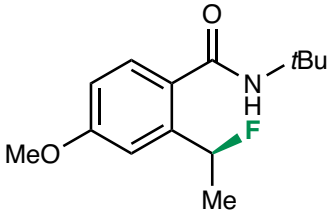

2g
(36 ± 3) TTN
21% yield, 90:10 e.r.
2g:**3g** = 40:60

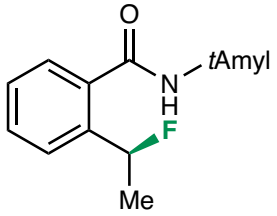

2h
(500 ± 10) TTN
76% yield, 95:5 e.r.
2h:**3h** = 98:2

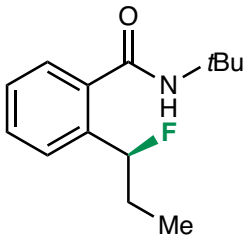

2i
(299 ± 2) TTN
91% yield, 95:5 e.r.
2i:**3i** = 98:2

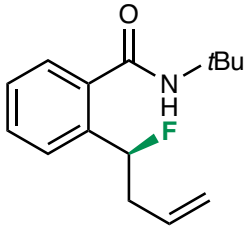

2j
(102 ± 1) TTN
74% yield, 96:4 e.r.
2j:**3j** = 99:1

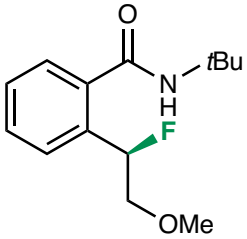

2k
(37 ± 1) TTN
32% yield, 97:3 e.r.
2k:**3k** = 68:32

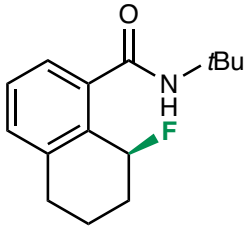

2l
(64 ± 2) TTN
37% yield, 81:19 e.r.
2l:**3l** = 93:7

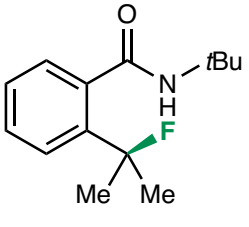

2m
(273 ± 2) TTN
79% yield
2m:**3m** = 95:5

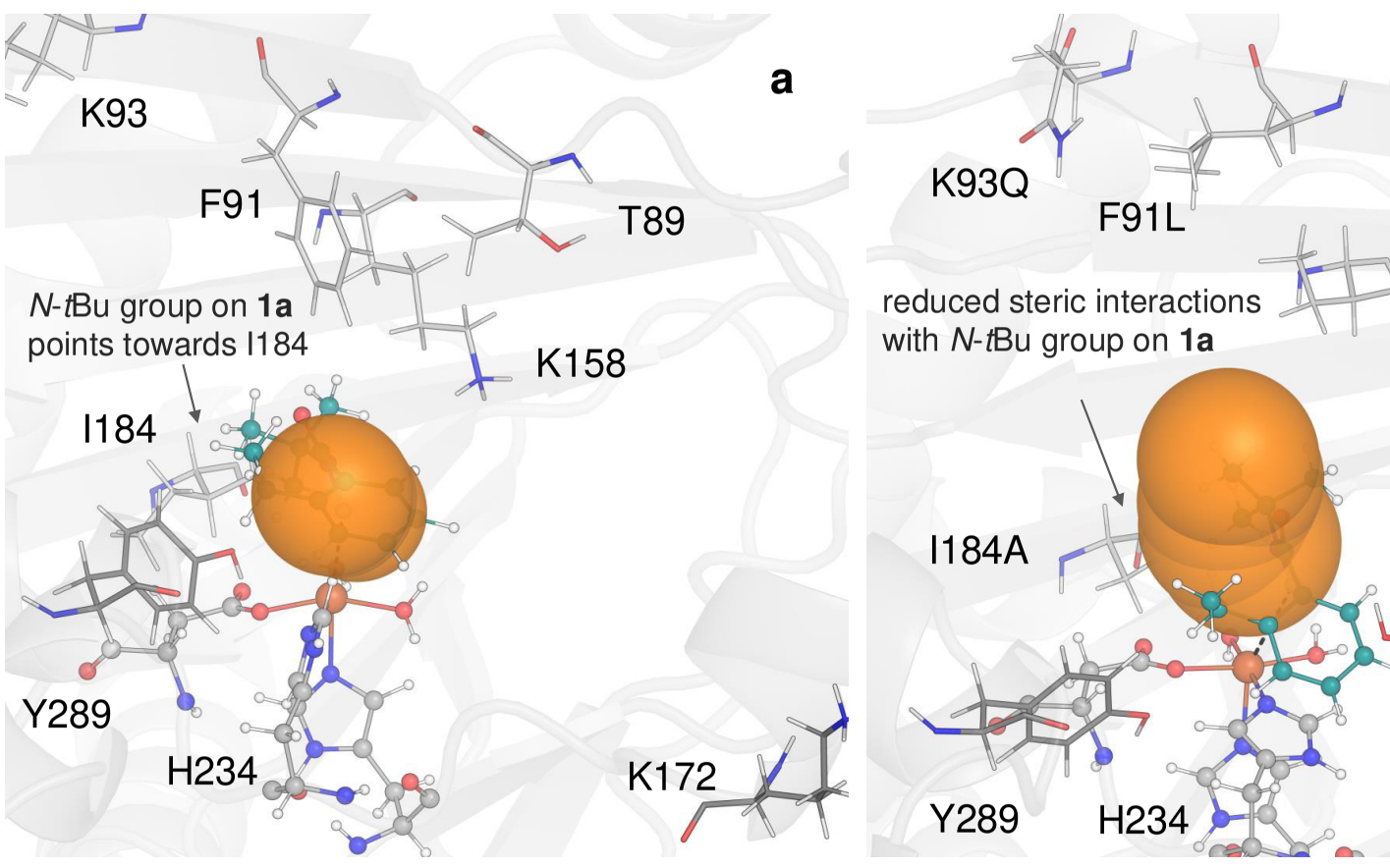
a
K93
F91
T89
K158
N-tBu group on 1a
points towards I184
I184
Y289
H234
K172
K93Q
F91L
reduced steric interactions
with N-tBu group on 1a
I184A
Y289
H234

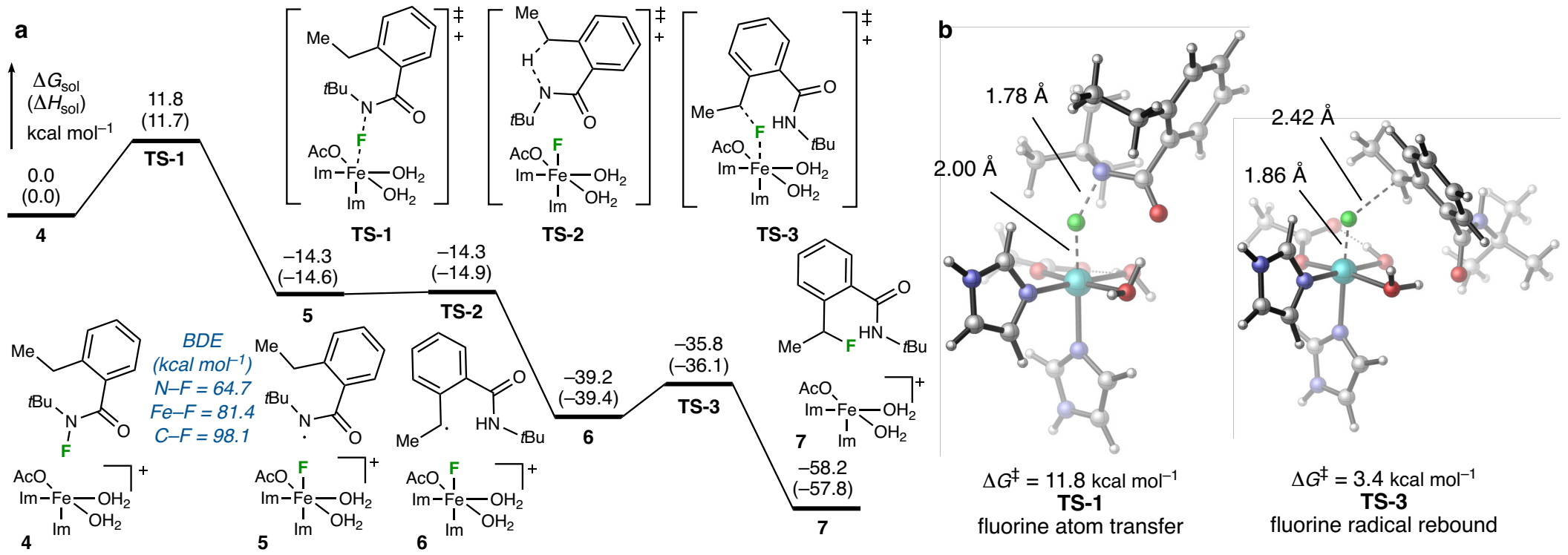
a
ΔGsol
(ΔHsol)
kcal mol−1
0.0
(0.0)
4
11.8
(11.7)
TS-1
−14.3
(−14.6)
5
−14.3
(−14.9)
TS-2
−39.2
(−39.4)
6
−35.8
(−36.1)
TS-3
−58.2
(−57.8)
7
BDE
(kcal mol−1)
N–F = 64.7
Fe–F = 81.4
C–F = 98.1
b
1.78 Å
2.00 Å
2.42 Å
1.86 Å
ΔG‡ = 11.8 kcal mol−1
TS-1
fluorine atom transfer
ΔG‡ = 3.4 kcal mol−1
TS-3
fluorine radical rebound

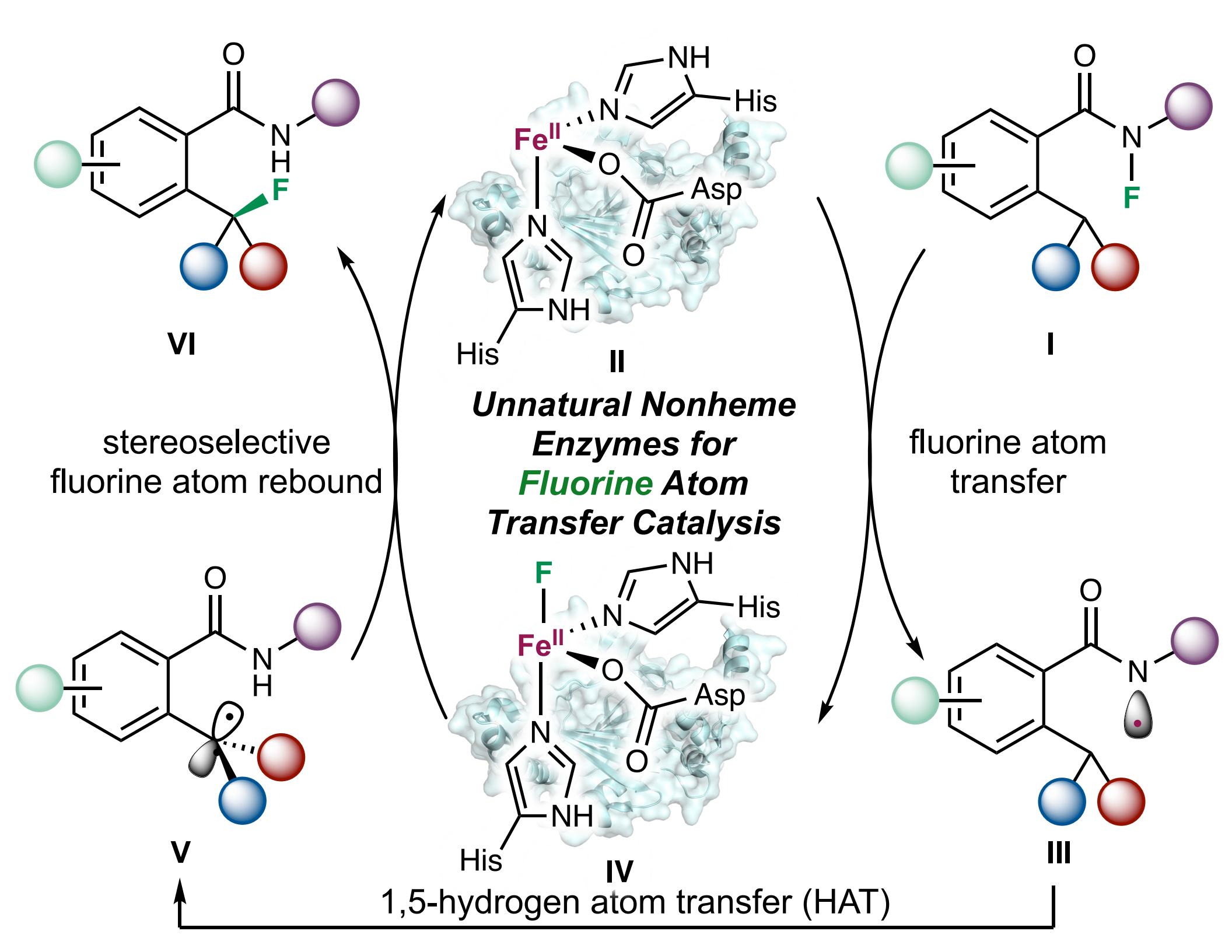
VI
II
I
stereoselective
fluorine atom rebound
Unnatural Nonheme
Enzymes for
Fluorine Atom
Transfer Catalysis
fluorine atom
transfer
V
IV
III
1,5-hydrogen atom transfer (HAT)